HHS Public Access

Author manuscript

Am J Ophthalmol. Author manuscript; available in PMC 2022 October 01.

Published in final edited form as:

Am J Ophthalmol. 2021 October ; 230: 156–165. doi:10.1016/j.ajo.2021.05.019.

Hemiretinal Asymmetry in Peripapillary Vessel Density in Healthy, Glaucoma Suspect, and Glaucoma Eyes

Kendra L. Hong[1], **Bruce Burkemper**[1], **Anna L. Urrea**[1], **Brenda R. Chang**[1], **Jae C. Lee**[1], **Vivian H. LeTran**[1], **Zhongdi Chu**[2], **Xiao Zhou**[2], **Benjamin Y. Xu**[1], **Brandon J. Wong**[1], **Brian J. Song**[1], **Xuejuan Jiang**[1], **Ruikang K. Wang**[2], **Rohit Varma**[3], **Grace M. Richter**[1]

[1]Department of Ophthalmology, USC Roski Eye Institute, Keck School of Medicine of University of Southern California, 1450 San Pablo St, Los Angeles, CA 90033, United States.

[2]Department of Bioengineering, University of Washington, Box 355061, 3720 15th Ave NE, Seattle, WA 98195, United States.

[3]Southern California Eye Institute, CHA Hollywood Presbyterian Medical Center, 1300 Vermont Ave, Los Angeles, CA 90027, United States.

Abstract

Purpose: To investigate hemiretinal asymmetry in radial peripapillary capillary vessel area density (VAD) of healthy, glaucoma suspect, and glaucoma eyes of varying severity and its diagnostic utility for glaucoma.

Design: Population-based, cross-sectional study.

Methods: 6×6-mm optic disc scans were collected on optical coherence tomography angiography (OCTA) to obtain VAD and on OCT to measure circumpapillary retinal nerve fiber layer (RNFL) thickness. Hemiretinal difference in VAD (hdVAD) was defined as the absolute difference between superior and inferior hemiretinal VAD. Age-adjusted multivariable linear regression of hdVAD on glaucoma severity was performed. Area under curves (AUCs) were calculated from predicted probabilities generated by multiple logistic regression of glaucoma severity on age-adjusted single and combined parameters.

Results: 1043 eyes of 1043 participants (587 healthy, 270 suspect, 67 mild, 54 moderate, 65 severe glaucoma) were included. After age adjustment, mean hdVAD was similar between healthy and suspect ($P = 0.225$), higher in mild versus suspect ($P < 0.001$), higher in moderate versus mild ($P = 0.018$), but lower in severe versus moderate ($P = 0.001$). AUCs of hdVAD were highest for discriminating mild (0.685) and moderate (0.681) glaucoma from healthy. Combining hdVAD

Corresponding Author: Grace M. Richter, USC Roski Eye Institute, Keck Medicine of University of Southern California, 1450 San Pablo St, Suite 3700, Los Angeles, CA 90033, Phone: 323-442-6421, Fax: 323-442-6413, grace.richter@med.usc.edu.

Meeting Presentations: Parts of the data in the manuscript were previously presented as a virtual abstract and oral presentation at the Association for Research in Vision and Ophthalmology Annual Conference 2020 and 2021.

Supplemental Material available at AJO.com

and global RNFL (gRNFL) yielded the highest AUCs of all parameters for mild (0.817) and any POAG (0.859) and resulted in significantly better diagnostic accuracy than either hdVAD or gRNFL alone ($P < 0.05$ for all comparisons).

Conclusions: hdVAD is higher in early glaucoma and may help with early detection when damage is focal, but its diagnostic ability appears less robust in advanced glaucoma when damage is diffuse.

Table of Contents Statement

Primary open-angle glaucoma (POAG) often begins with focal damage in one hemiretina. This cross-sectional study investigates hemiretinal difference in peripapillary vessel area density (hdVAD) in healthy, glaucoma suspect, and POAG eyes at various stages, and its diagnostic ability for POAG. hdVAD is highest in early POAG when damage is more focal and has good diagnostic ability when combined with retinal nerve fiber layer thickness for distinguishing mild and any POAG eyes from healthy eyes.

INTRODUCTION

Primary open-angle glaucoma (POAG) is a progressive optic neuropathy and a leading cause of blindness.[1] However, patients often remain asymptomatic until late stages when functional visual field loss is more debilitating.[1] Current standards of detecting early glaucomatous changes have limitations: stereoscopic disc examination may not detect subtle nerve changes,[2] and up to 30–50% of retinal ganglion cells may be lost before defects are detectable by visual field testing.[1] Optical coherence tomography (OCT) is a widespread diagnostic tool for glaucoma[3] that measures retinal nerve fiber layer (RNFL) thickness and ganglion cell-inner plexiform layer thickness to assess ganglion cell axonal loss, but it is limited in its ability to detect early disease.[4–6] Although optical coherence tomography angiography (OCTA) effectively quantifies the reduction in microvasculature in glaucoma[7–11] before visual field loss occurs,[12] its use in glaucoma diagnosis has yet to be optimized.[11,13]

Early detection and treatment of POAG are essential to prevent irreversible damage.[1,14,15] Because POAG begins with focal changes to RNFL thickness,[16–20] microvasculature,[21–28] and visual field,[28,29] hemispheric asymmetry in these parameters may be useful for characterizing early glaucomatous damage. Hemispheric asymmetry measurements may also be advantageous over global measurements that are compared to a normative database because confounding effects related to factors such as race/ethnicity can be avoided when the healthy region of the patient's eye is used as a control to compare to the diseased region of the same eye.[30]

Hemispheric asymmetry can be measured both functionally and structurally via visual field loss and RNFL, respectively. The glaucoma hemifield test identifies differences in visual field loss between the superior and inferior hemifields to help detect early glaucoma,[29] but the test has low specificity and repeatability.[31] Hemispheric asymmetry in RNFL[16] and ganglion cell-inner plexiform layer[17–20] thickness on OCT reflects regional differences in ganglion cell loss and has demonstrated some utility for early glaucoma detection.[30,32]

Presently, there is limited data on hemispheric asymmetry in peripapillary vessel density in glaucoma as measured by OCTA. While focal perfusion loss is correlated with RNFL thinning and visual field loss in early glaucoma,[10,27,28] Chen et al. reported that the normal retinal hemisphere in glaucomatous eyes with hemifield visual field loss had RNFL thickness comparable to normal eyes, albeit with reduced microvasculature.[23] This suggests that focal microvascular changes may occur prior to RNFL thickness changes. Additionally, several studies have demonstrated that early glaucoma can be characterized by small regions of microvascular reduction,[21–28] which may lead to a perfusion difference between the superior and inferior hemiretinas. To assess the magnitude of perfusion difference at each glaucoma severity level, we derived a novel asymmetry parameter, hemiretinal difference in peripapillary vessel area density (hdVAD), which is defined as the absolute difference between two standard OCTA measurements: superior and inferior hemiretinal peripapillary vessel area density (VAD). The hypothesis of our study was that this novel hemiretinal microvascular asymmetry parameter may be uniquely suited for detecting early glaucoma.

The purpose of the study was to use OCTA to investigate hdVAD of healthy, glaucoma suspect, and POAG eyes at various stages ranging from mild to severe, and to assess its potential in detecting early glaucomatous damage.

METHODS

Study population:

Participants aged 40 and older were recruited from 2 sources: 1) self-identified African Americans residing in Inglewood, California who participated in the African American Eye Disease Study (AFEDS) from February 2016 to April 2018,[33] and 2) patients who presented to the glaucoma service clinic at the University of Southern California (USC) Roski Eye Institute from March 2016 to January 2020. Both research protocols were approved by the USC Health Sciences Campus Institutional Review Board and implemented in accordance with the Declaration of Helsinki and Health Insurance Portability and Accountability Act regulations. Written informed consent was obtained from all participants after an explanation of the nature and intent of the study.

Clinical Assessment:

Systemic information collected included age, sex, race/ethnicity, diagnosis of hypertension, and diagnosis of diabetes mellitus. Each participant underwent a complete ocular examination, including gonioscopy, dilated fundoscopy, intraocular pressure (IOP) measurements using Goldmann applanation tonometry, visual field evaluation with Swedish Interactive Threshold Algorithm (SITA) Standard 24–2 test (Carl Zeiss Humphrey Field Analyzer II 750), OCT imaging (Cirrus 5000 HD-OCT; Carl Zeiss Meditec, Dublin, CA, USA), and OCTA imaging (Cirrus 5000 HD-OCT with Angioplex; Carl Zeiss Meditec). Visual field mean deviation (MD) and pattern standard deviation (PSD) were derived from the SITA Standard 24–2 test. The OCT system calculated RNFL thickness along a 3.4-mm diameter circle centered on the middle of the optic nerve head (ONH) using the Cirrus AutoCenter™ function (Zeiss).

A diagnosis of healthy, glaucoma suspect, or POAG at each stage (mild, moderate, and severe) was based on a comprehensive clinical assessment by an ophthalmologist. All eyes had open angles on gonioscopy. Healthy participants were recruited from AFEDS, a population-based study that included many without ocular diseases, and from the USC glaucoma clinic, where participants were deemed to be not at risk for glaucoma after a comprehensive evaluation. Each healthy eye met the following criteria: non-glaucomatous optic disc, no features characteristic of glaucoma suspect, and no ocular diseases that could affect retinal perfusion and visual field such as age-related macular degeneration, severe non-proliferative diabetic retinopathy, proliferative diabetic retinopathy, and macular edema. Glaucoma suspect eyes had clinical features that were potentially consistent with or characteristic of glaucoma but not definitive enough to support a diagnosis of glaucoma. These features included any of the following: IOP > 21 mm Hg, a symmetric large cup-to-disc ratio (CDR) ≥ 0.5 without an optic disc or visual field abnormality characteristic of or compatible with glaucoma, marked IOP asymmetry (≥ 5 mm Hg) between eyes, and CDR asymmetry ≥ 0.2 without visual field defect. POAG eyes had clinical features that were consistent with or characteristic of POAG, including defects in the optic nerve rim (such as notching or localized thinning) and visual field (Humphrey Visual Field 24–2; Zeiss). POAG staging was based on the International Classification of Disease and Related Health Problems version 10 (ICD-10) glaucoma staging definitions.[34]

OCTA images were excluded if participants had a history of retinal or non-glaucomatous optic nerve disease, narrow angle, angle-closure glaucoma, secondary open angle glaucoma including pseudoexfoliation and pigmentary glaucoma, high myopia (< −8.00D), or high hyperopia (> +2.50D). Exclusion criteria for images also included segmentation error (as determined by review of B-scans), poor signal strength (SS) (<7/10), and poor quality based on a standardized image quality grading algorithm that took into account motion artifacts, decentration (defined as the middle of the ONH being ≥ 0.8 mm from the center of the image), and media opacities such as vitreous floaters. For each participant, the eye with the highest image quality score was selected for analysis. Visual field test results were excluded if unreliable (> 33% fixation loss, > 15% false positive error, or > 33% false negative error).

OCTA Image Analysis:

Automated optical microangiography (OMAG) software (Carl Zeiss Meditec Inc.) precisely segmented the RNFL and created two-dimensional 6×6-mm *en face* representations of the perfused radial peripapillary capillaries (RPC) within the RNFL. A custom quantification software with an interactive interface in MATLAB (R2017a; MathWorks Inc, Natick, MA) quantified perfused retinal vascular density and morphology for the segmented RPC *en face* image. OCTA images were converted into binary vessel maps using global thresholding, Hessian filter, and adaptive threshold. The avascular portion of the ONH, which was defined as a circular area of 1 mm from the middle of the ONH, was selected to establish a baseline for background noise for global thresholding before being excluded from quantification. Large vessels, defined as those greater than 32 μm, were also excluded from quantification. Quantification was limited to a circular area of radius 2.8 mm, centered in the middle of the ONH. The area of analysis was further divided into hemispheres and quadrants. From the

circular binary vessel map output, VAD was calculated as the ratio of the total number of pixels occupied by vasculature to the total number of pixels in the circular vessel map.[35]

Global and Asymmetry Parameters:

Global VAD (gVAD) was defined as the VAD of a 2.8-mm radius circle centered on the ONH in the 6×6-mm RPC image, minus the ONH and large vessels. hdVAD was defined as the absolute difference between the superior and inferior hemiretinal peripapillary VAD of the 2.8-mm radius circle. Quadrant difference in VAD (qdVAD) was defined as the absolute difference between the superior and inferior quadrant peripapillary VAD of the 2.8-mm radius circle.

Global RNFL thickness (gRNFL) was defined as the average RNFL thickness along a 3.4-mm diameter circle centered on the ONH. Quadrant difference in RNFL thickness (qdRNFL) was defined as the absolute difference between the superior and inferior quadrant RNFL thickness along the 3.4-mm diameter circle.

Statistical Analyses:

SAS 9.4 software (SAS Institute Inc., Cary, NC, USA) was used for all analyses. P-values < 0.05 were considered statistically significant. Logistic regression of diagnostic groups on demographic characteristics, with age as a covariate, assessed for significant differences in demographic characteristics between each pair of diagnostic groups.

Multivariable linear regressions of ocular parameters (i.e. VAD, RNFL, visual field MD) on diagnostic groups were performed, with age as a covariate, to determine if the mean values of ocular parameters differed significantly between diagnostic groups. The diagnostic accuracy of these ocular parameters was quantified by area under curves (AUCs). AUCs were determined from predicted probabilities of diagnosis calculated from multiple logistic regression models in which the binary outcome was diagnosis (with healthy serving as the reference group) and the predictor variable was either a single parameter or a combination of parameters. Age was partialled out of the parameters in order to control for age without including it as a covariate in the models. Therefore, AUCs could be estimated without the upward bias that would otherwise result had age been included as a covariate, given the positive correlation between age and each outcome. DeLong's test was used to determine the statistical significance of differences in AUCs from various models, thus identifying parameters with the greatest diagnostic accuracy. Locally weighted scatterplot smoothing (LOWESS) plots were generated to visualize the relationship between predicted values of hdVAD and other ocular parameters, including measures of function (visual field MD and PSD) and structure (gRNFL).

RESULTS

Of the 3046 participants aged 40 and older, 7666 OCTA images were obtained. 611 images were excluded due to having a SS < 7/10; 3562 images were excluded due to having poor image quality caused by motion artifacts, flashes and floaters, faded capillaries, or missing data; 708 images were excluded due to participants having ocular conditions such as retinal or non-glaucomatous optic nerve disease, angle closure glaucoma, secondary glaucoma,

high myopia, or high hyperopia; 174 images were excluded due to bilateral OD and OS imaging or repeat imaging of the same eye. The remaining 1043 images from 1043 eyes and 1043 participants were classified as healthy (587), glaucoma suspect (270), or “any POAG” (186), and the latter category was further subdivided into mild (67), moderate (54), and severe (65) POAG.

Table 1 shows that among the healthy, suspect, and any POAG groups, there were significant between-group differences in gender, hypertension, and diabetes even when age was controlled. However, these demographic variables were not significant when included as covariates in our age-adjusted multivariable regression models of ocular parameters on diagnostic groups and did not confound the results from these models to any appreciable extent, as demonstrated by similar β-values with and without the variables as covariates (data not shown). In comparison to the healthy and suspect groups, the any POAG group had a higher mean CDR ($P < 0.001$ for both comparisons), lower mean visual field MD ($P < 0.001$ for both), and higher mean PSD ($P < 0.001$ for both). Between-group differences in IOP were not significant.

Figure 1 demonstrates qualitative focal vascular attenuation in eyes with mild POAG and increasingly multifocal and diffuse vascular attenuation in eyes with more advanced POAG. Similarly, mean predicted values of several VAD and RNFL parameters decreased with more severe disease (Table 2).

Table 2 shows that age-adjusted mean predicted asymmetry values of peripapillary VAD, including hdVAD and qdVAD, were significantly higher in mild, moderate, and severe POAG compared to healthy. Figure 2 and Supplemental Figure 1A demonstrate the distributions of age-adjusted predicted hdVAD and qdVAD, respectively, across diagnostic groups. Mean predicted hdVAD was not significantly different between healthy and suspect ($\beta = 0.001$, $P = 0.225$), but was significantly higher in mild POAG versus suspect ($\beta = 0.003$, $P < 0.001$) and in moderate versus mild POAG ($\beta = 0.004$, $P = 0.018$). In contrast, mean predicted hdVAD was significantly lower in severe versus moderate POAG ($\beta = -0.004$, $P = 0.001$). Similar magnitudes and directions of between-group differences were observed for qdVAD (Supplemental Figure 1A). Corresponding between-group differences in intra-eye asymmetry of RNFL, as measured by qdRNFL, were not significant (Supplemental Figure 1B; $P > 0.05$ for all comparisons).

Table 2 demonstrates that for mean predicted hdVAD, mild POAG was the least severe group in which a significant difference from healthy was observed ($P < 0.001$). Between healthy and mild POAG, we also found significant differences in several RNFL and VAD parameters, but not in mean predicted visual field MD ($P = 0.465$) or PSD ($P = 0.822$). Furthermore, in Figures 3A and 3B, we observed that at early stages of POAG when eyes have high MD and low PSD in visual field testing, there is a qualitative peak in predicted hdVAD in the LOWESS regression curve for any POAG. Similarly, qualitatively higher predicted hdVAD in the any POAG LOWESS regression curve was observed where gRNFL values of the healthy, suspect, and any POAG groups overlap in early POAG (Supplemental Figure 2).

After finding evidence for between-group parameter differences using models in which ocular parameters served as outcome variables, we ran a series of models with the ocular parameters serving as predictor variables to determine their diagnostic accuracy, as measured with AUC; these results are presented in Table 3. AUCs of hdVAD were qualitatively highest for mild (0.685) and moderate (0.681) POAG (versus 0.517 for suspect, 0.594 for severe POAG, 0.657 for any POAG), and AUCs of qdVAD were qualitatively highest for moderate (0.725) POAG (versus 0.519 for suspect, 0.611 for mild POAG, 0.630 for severe POAG, 0.648 for any POAG). Since gRNFL yielded the highest AUCs for discriminating each diagnostic group from healthy (Table 3), gRNFL was included with VAD parameters as predictors to optimize diagnostic accuracy. Of all parameters, the combination of gRNFL and hdVAD had the highest AUCs, which were significantly greater versus AUCs for gRNFL alone for discriminating mild (0.818 for combination versus 0.793 for gRNFL, P = 0.037) and any POAG (0.859 for combination versus 0.847 for gRNFL, P = 0.049) from healthy. No other combinations of two parameters yielded an AUC that was statistically significantly higher than *either* the AUC of the combined hdVAD and gRNFL model *or* the AUC of gRNFL for discriminating a particular diagnostic group from healthy (Table 3).

DISCUSSION

We evaluated hdVAD in healthy, glaucoma suspect, and POAG eyes in mild, moderate, and severe stages of the disease. Of all diagnostic groups, mean predicted hdVAD was highest for mild and moderate POAG. hdVAD was most helpful in the diagnosis of early POAG, and the combination of hdVAD and gRNFL yielded the best diagnostic accuracy of all parameter permutations for mild and any POAG. These data suggest that efforts to analyze this novel hemiretinal peripapillary vessel density asymmetry parameter may enhance the clinician's ability to detect early and focal glaucomatous damage.

The finding of hemiretinal peripapillary microvascular asymmetry in early POAG is consistent with evidence that early glaucomatous damage is focal and deep,[21–28,36] and this pattern of early damage may serve as the basis for perfusion differences between the superior and inferior hemiretinas in early POAG. As POAG progresses, damage likely becomes multifocal and diffuse[27,28,36,37] such that differences between hemiretinas become smaller again in the severe stages of the disease. This is reflected in the diagnostic accuracy of hdVAD when discriminating each diagnostic group from healthy: AUCs were highest for mild and moderate POAG but lower for suspect and severe POAG. Therefore, hdVAD may be most effective in detecting early stages of the disease before glaucomatous damage becomes multifocal or diffuse.

The AUCs of hdVAD suggest that it is most useful in diagnosing early POAG, and combining hdVAD with gRNFL yielded the highest diagnostic accuracy for mild and any POAG. This supports the possibility that glaucomatous damage, even in its early stages, may be characterized by both focal microvascular damage and global structural damage. A diffuse RNFL thinning in early POAG has been observed in previous studies,[38,39] and these findings may explain the lack of RNFL quadrant asymmetry in our study. Nevertheless, mean RNFL has low sensitivity in detecting early POAG,[4–6,13] which is often characterized

by focal changes[21–28] to which hdVAD may be more sensitive. Specifically, in early POAG when gRNFL is within healthy and suspect ranges, the LOWESS regression curve for any POAG (Supplemental Figure 2) shows a high hdVAD, suggesting that hemiretinal microvascular asymmetry may serve as a valuable complement to measures of structural damage in early POAG detection.

Because significant differences between healthy and mild POAG were observed in several VAD and RNFL parameters but not in visual field parameters, damage to microvasculature and structure may precede functional loss. Additionally, in early POAG when eyes have undergone very mild visual field changes, we observed apparent peaks in hdVAD in the any POAG LOWESS regression curves (Figures 3A and 3B), suggesting that early focal changes to microvasculature may occur *before* significant functional changes, irrespective of how glaucoma staging is defined. Future longitudinal studies can help elucidate the temporal relationship of microvasculature, structure, and visual field changes.

A benefit of using VAD asymmetry over standard VAD measurements (i.e. global, hemiretinal, and quadrant VAD) is that within-eye comparisons allow the healthy region of a patient's peripapillary retina to serve as its own control when assessing for focal damage so that clinicians do not have to rely on normative databases.[40,41] However, the results of hemiretinal microvascular asymmetry analyses are meaningful only if the following two assumptions are met: 1) eyes have no hemiretinal microvascular asymmetries at baseline, which the healthy eyes in our study data demonstrated, and 2) although glaucomatous microvascular damage may be diffuse at later stages, it develops focally in early stages of the disease such that the peripapillary retina contains healthy regions that can serve as a control for comparison. Even though glaucomatous damage has been shown to begin focally,[21–28] evidence suggests that the damage does not occur consistently in one particular hemiretina or quadrant over the other: some studies report initial damage in the inferior region,[27,39,42–45] while others report it in the superior region.[46–48] Therefore, superior or inferior VAD alone is not particularly sensitive, providing another reason to favor VAD asymmetry for early detection of glaucoma.

The present study has several limitations. First, most of our healthy participants (>99%) were recruited from AFEDS, a study comprised entirely of African Americans. In contrast, our POAG participants were recruited from both AFEDS and the USC glaucoma service clinic, the latter comprising of participants with a large degree of ethnic diversity characteristic of the greater Los Angeles area. Nousome et al. recently demonstrated that RNFL thickness does vary by ethnicity,[49] and the same may apply to peripapillary VAD. However, there have been no studies demonstrating that hemiretinal asymmetry in RNFL or VAD varies by ethnicity, and hemiretinal asymmetry may be advantageous given Nousome et al.'s finding because the control for comparison is the healthy portion of the peripapillary retina, rather than normative means that can vary across ethnicity. Nevertheless, to gauge the extent to which our results may have been confounded by an unequal ethnic distribution across groups of increasing severity, we performed a sensitivity analysis restricted to African Americans participants. Although the smaller cohort size yielded less powerful statistical tests, we obtained similar results in terms of both magnitude and direction of between-group differences and accompanying p-values (data not shown). We thus concluded that ethnicity

did not confound our results to any appreciable degree. Secondly, a limitation to our study's sub-analysis of visual fields is that we did not exclude for lens rim artifacts, inattention, or obstruction of the visual field axis, such as droopy eyelid. Lastly, while the 6×6-mm OCTA scan size was used in this study and has been used in several other glaucoma OCTA studies,[26,27,42] the 4.5×4.5-mm OCTA size has demonstrated better diagnostic ability in mild POAG.[50] Future studies can elucidate if the greater resolution of the 4.5×4.5-mm scan size can increase the diagnostic ability of hdVAD, especially for early POAG.

CONCLUSION

We investigated hdVAD, a novel hemiretinal peripapillary vessel density asymmetry parameter derived from OCTA images, in healthy, glaucoma suspect, and POAG eyes of varying severity. hdVAD is highest in early POAG when damage is more focal but becomes lower in later stages of disease when damage is more multifocal and diffuse. hdVAD appears to be most helpful in the diagnosis of early POAG and has a high degree of sensitivity and specificity when combined with gRNFL for distinguishing eyes with mild or any POAG from healthy eyes. Future studies should evaluate peripapillary perfusion longitudinally to investigate potential temporal relationships in structure, microvasculature, and visual field dynamics. Ultimately, these studies can help us understand the clinical utility of OCTA and its ability to supplement other clinical measures in the diagnosis of early glaucoma.

Supplementary Material

Refer to Web version on PubMed Central for supplementary material.

ACKNOWLEDGEMENTS

Funding/Support:

National Institutes of Health grants (Bethesda, MD; K23EY027855-01, G.M.R.; U10EY023575, R.V.; R01EY028753, R.K.W., K23EY029763, B.Y.X.), American Glaucoma Society Young Clinician Scientist grant (San Francisco, CA; G.M.R.), an unrestricted grant to the USC Department of Ophthalmology from Research to Prevent Blindness (New York, NY), and Carl Zeiss Meditec (Dublin, CA; SD-OCTA device).

Financial Disclosures:

R.K.W is a consultant of and receives a grant from Carl Zeiss Meditec, and he holds a patent on the SD-OCTA device from Carl Zeiss Meditec. G.M.R. has access to an SD-OCTA research device provided by Carl Zeiss Meditec Inc. The remaining authors declare no financial disclosures.

Other Acknowledgements:

The African American Eye Disease Study Group, University of Southern California, Los Angeles, CA: Rohit Varma, MD, MPH; Roberta McKean-Cowdin, PhD; Mina Torres, MS; Alicia Fairbrother-Crisp, MPH; Farzana Choudhury MBBS, MS, PhD; Xuejuan Jiang, PhD; Bruce Burkemper, PhD, MS; Tengiz Adamashvili; Carlos Lastra, MD; Elizabeth Corona; YuPing Wang, COT; Jacqueline Douglass, Jaimie Barrera; Judith Linton.

REFERENCES

1. Weinreb RN, Aung T, Medeiros FA. The pathophysiology and treatment of glaucoma: a review. JAMA. 2014;311(18):1901–1911. doi:10.1001/jama.2014.3192 [PubMed: 24825645]
2. Tatham AJ, Weinreb RN, Zangwill LM, Liebmann JM, Girkin CA, Medeiros FA. The relationship between cup-to-disc ratio and estimated number of retinal ganglion cells. Invest Ophthalmol

Vis Sci. 2013;54(5):3205–3214. Published 2013 May 7. doi:10.1167/iovs.12-11467 [PubMed: 23557744]

3. Tatham AJ, Medeiros FA. Detecting Structural Progression in Glaucoma with Optical Coherence Tomography. Ophthalmology. 2017;124(12S):S57–S65. doi:10.1016/j.ophtha.2017.07.015 [PubMed: 29157363]
4. Dong ZM, Wollstein G, Schuman JS. Clinical Utility of Optical Coherence Tomography in Glaucoma. Invest Ophthalmol Vis Sci. 2016;57(9):OCT556–OCT567. doi:10.1167/iovs.16-19933 [PubMed: 27537415]
5. Leite MT, Zangwill LM, Weinreb RN, et al. Effect of disease severity on the performance of Cirrus spectral-domain OCT for glaucoma diagnosis. Invest Ophthalmol Vis Sci. 2010;51(8):4104–4109. doi:10.1167/iovs.09-4716 [PubMed: 20335619]
6. Nouri-Mahdavi K, Hoffman D, Tannenbaum DP, Law SK, Caprioli J. Identifying early glaucoma with optical coherence tomography. Am J Ophthalmol. 2004 2;137(2):228–35. doi: 10.1016/j.ajo.2003.09.004. [PubMed: 14962410]
7. Akil H, Huang AS, Francis BA, Sadda SR, Chopra V. Retinal vessel density from optical coherence tomography angiography to differentiate early glaucoma, pre-perimetric glaucoma and normal eyes. PLoS One. 2017;12(2):e0170476. Published 2017 Feb 2. doi:10.1371/journal.pone.0170476 [PubMed: 28152070]
8. Jia Y, Morrison JC, Tokayer J, et al. Quantitative OCT angiography of optic nerve head blood flow. Biomed Opt Express. 2012;3(12):3127–3137. doi:10.1364/BOE.3.003127 [PubMed: 23243564]
9. Scripsema NK, Garcia PM, Bavier RD, et al. Optical Coherence Tomography Angiography Analysis of Perfused Peripapillary Capillaries in Primary Open-Angle Glaucoma and Normal-Tension Glaucoma. Invest Ophthalmol Vis Sci. 2016;57(9):OCT611–OCT620. doi:10.1167/iovs.15-18945 [PubMed: 27742922]
10. Van Melkebeke L, Barbosa-Breda J, Huygens M, Stalmans I: Optical Coherence Tomography Angiography in Glaucoma: A Review. Ophthalmic Res 2018;60:139–151. doi: 10.1159/000488495 [PubMed: 29794471]
11. Yarmohammadi A, Zangwill LM, Diniz-Filho A, et al. Optical Coherence Tomography Angiography Vessel Density in Healthy, Glaucoma Suspect, and Glaucoma Eyes. Invest Ophthalmol Vis Sci. 2016;57(9):OCT451–OCT459. doi:10.1167/iovs.15-18944 [PubMed: 27409505]
12. Yarmohammadi A, Zangwill LM, Manalastas PIC, et al. Peripapillary and Macular Vessel Density in Patients with Primary Open-Angle Glaucoma and Unilateral Visual Field Loss. Ophthalmology. 2018;125(4):578–587. doi:10.1016/j.ophtha.2017.10.029 [PubMed: 29174012]
13. Rao HL, Pradhan ZS, Suh MH, Moghimi S, Mansouri K, Weinreb RN. Optical Coherence Tomography Angiography in Glaucoma. J Glaucoma. 2020 4;29(4):312–321. doi: 10.1097/IJG.0000000000001463. [PubMed: 32053551]
14. Leske MC, Heijl A, Hyman L, Bengtsson B. Early Manifest Glaucoma Trial: design and baseline data. Ophthalmology. 1999 11;106(11):2144–53. doi: 10.1016/s0161-6420(99)90497-9. [PubMed: 10571351]
15. Musch DC, Lichter PR, Guire KE, Standardi CL. The Collaborative Initial Glaucoma Treatment Study: study design, methods, and baseline characteristics of enrolled patients. Ophthalmology. 1999 4;106(4):653–62. doi: 10.1016/s0161-6420(99)90147-1. [PubMed: 10201583]
16. Gardiner SK, Fortune B, Demirel S. Localized Changes in Retinal Nerve Fiber Layer Thickness as a Predictor of Localized Functional Change in Glaucoma. Am J Ophthalmol. 2016;170:75–82. doi:10.1016/j.ajo.2016.07.020 [PubMed: 27491698]
17. Inuzuka H, Kawase K, Yamada H, Oie S, Kokuzawa S, Yamamoto T. Macular ganglion cell complex thickness in glaucoma with superior or inferior visual hemifield defects. J Glaucoma. 2014;23(3):145–149. doi:10.1097/IJG.0b013e31826a7e20. [PubMed: 24042125]
18. Kim HS, Yang H, Lee TH, Lee KH. Diagnostic Value of Ganglion Cell-Inner Plexiform Layer Thickness in Glaucoma With Superior or Inferior Visual Hemifield Defects. J Glaucoma. 2016;25(6):472–476. doi:10.1097/IJG.0000000000000285. [PubMed: 26164145]
19. Lin PW, Chang HW, Lai IC, Tsai JC, Poon YC. Intraocular retinal thickness asymmetry in early stage of primary open angle glaucoma and normal tension glaucoma. Int J

Ophthalmol. 2018;11(8):1342–1351. Published 2018 Aug 18. doi:10.18240/ijo.2018.08.15 [PubMed: 30140639]

20. Yamada H, Hangai M, Nakano N, et al. Asymmetry Analysis of Macular Inner Retinal Layers for Glaucoma Diagnosis. Am J Ophthalmol. 2014;158:1318–1329. doi:10.1016/j.ajo.2014.08.040 [PubMed: 25194230]
21. Akagi T, Iida Y, Nakanishi H, et al. Microvascular Density in Glaucomatous Eyes With Hemifield Visual Field Defects: An Optical Coherence Tomography Angiography Study. Am J Ophthalmol. 2016;168:237–249. doi: 10.1016/j.ajo.2016.06.009 [PubMed: 27296492]
22. Chen A, Liu L, Wang J, et al. Measuring Glaucomatous Focal Perfusion Loss in the Peripapillary Retina Using OCT Angiography. Ophthalmology. 2020;127(4):484–491. doi:10.1016/j.ophtha.2019.10.041 [PubMed: 31899032]
23. Chen CL, Bojikian KD, Wen JC, et al. Peripapillary Retinal Nerve Fiber Layer Vascular Microcirculation in Eyes With Glaucoma and Single-Hemifield Visual Field Loss. JAMA Ophthalmol. 2017;135(5):461–468. doi:10.1001/jamaophthalmol.2017.0261 [PubMed: 28358939]
24. Liu L, Jia Y, Takusagawa HL, et al. Optical Coherence Tomography Angiography of the Peripapillary Retina in Glaucoma. JAMA Ophthalmol. 2015;133(9):1045–1052. doi:10.1001/jamaophthalmol.2015.2225 [PubMed: 26203793]
25. Shoji T, Zangwill LM, Akagi T, et al. Progressive Macula Vessel Density Loss in Primary Open-Angle Glaucoma: A Longitudinal Study. Am J Ophthalmol. 2017;182:107–117. doi:10.1016/j.ajo.2017.07.011 [PubMed: 28734815]
26. Takusagawa HL, Liu L, Ma KN, et al. Projection-Resolved Optical Coherence Tomography Angiography of Macular Retinal Circulation in Glaucoma. Ophthalmology. 2017;124(11):1589–1599. doi:10.1016/j.ophtha.2017.06.002 [PubMed: 28676279]
27. Richter GM, Sylvester B, Chu Z, et al. Peripapillary microvasculature in the retinal nerve fiber layer in glaucoma by optical coherence tomography angiography: focal structural and functional correlations and diagnostic performance. Clin Ophthalmol. 2018;12:2285–2296. Published 2018 Nov 8. doi:10.2147/OPTH.S179816 [PubMed: 30510397]
28. Shin JW, Lee J, Kwon J, Choi J, Kook MS. Regional vascular density-visual field sensitivity relationship in glaucoma according to disease severity. Br J Ophthalmol. 2017 12;101(12):1666–1672. doi: 10.1136/bjophthalmol-2017-310180. Epub 2017 Apr 21. [PubMed: 28432111]
29. Asman P, Heijl A. Glaucoma Hemifield Test. Automated visual field evaluation. Arch Ophthalmol. 1992;110(6):812–819. doi:10.1001/archopht.1992.01080180084033 [PubMed: 1596230]
30. Khanal S, Davey PG, Racette L, Thapa M. Intraeye retinal nerve fiber layer and macular thickness asymmetry measurements for the discrimination of primary open-angle glaucoma and normal tension glaucoma. J Optom. 2016;9(2):118–125. doi:10.1016/j.optom.2015.10.002 [PubMed: 26652244]
31. Katz J, Quigley HA, Sommer A. Repeatability of the Glaucoma Hemifield Test in automated perimetry. Invest Ophthalmol Vis Sci. 1995;36(8):1658–1664. [PubMed: 7601645]
32. Lee SY, Lee EK, Park KH, Kim DM, Jeoung JW. Asymmetry Analysis of Macular Inner Retinal Layers for Glaucoma Diagnosis: Swept-Source Optical Coherence Tomography Study. PLoS One. 2016;11(10):e0164866. Published 2016 Oct 20. doi:10.1371/journal.pone.0164866 [PubMed: 27764166]
33. McKean-Cowdin R, Fairbrother-Crisp A, Torres M, et al. The African American Eye Disease Study: Design and Methods. Ophthalmic Epidemiol. 2018;25(4):306–314. doi:10.1080/09286586.2018.1454965 [PubMed: 29580111]
34. Parekh AS, Tafreshi A, Dorairaj SK, Weinreb RN. Clinical applicability of the International Classification of Disease and Related Health Problems (ICD-9) glaucoma staging codes to predict disease severity in patients with open-angle glaucoma. J Glaucoma. 2014 1;23(1):e18–22. doi:10.1097/IJG.0000000000000033. [PubMed: 24370808]
35. Chu Z, Lin J, Gao C, et al. Quantitative assessment of the retinal microvasculature using optical coherence tomography angiography. J Biomed Opt. 2016;21(6):66008. doi:10.1117/1.JBO.21.6.066008 [PubMed: 27286188]
36. Kumar RS, Anegondi N, Chandapura RS, Sudhakaran S, Kadambi SV, Rao HL, Aung T, Sinha Roy A. Discriminant Function of Optical Coherence Tomography Angiography to Determine

Disease Severity in Glaucoma. Invest Ophthalmol Vis Sci. 2016 11 1;57(14):6079–6088. doi: 10.1167/iovs.16-19984. [PubMed: 27820876]

37. Yarmohammadi A, Zangwill LM, Diniz-Filho A, et al. Relationship between Optical Coherence Tomography Angiography Vessel Density and Severity of Visual Field Loss in Glaucoma. Ophthalmology. 2016;123(12):2498–2508. doi:10.1016/j.ophtha.2016.08.041 [PubMed: 27726964]
38. Sullivan-Mee M, Ruegg CC, Pensyl D, Halverson K, Qualls C. Diagnostic precision of retinal nerve fiber layer and macular thickness asymmetry parameters for identifying early primary open-angle glaucoma. Am J Ophthalmol. 2013;156(3):567–577.e1. doi:10.1016/j.ajo.2013.04.037 [PubMed: 23810475]
39. Miki A, Medeiros FA, Weinreb RN, Jain S, He F, Sharpsten L, Khachatryan N, Hammel N, Liebmann JM, Girkin CA, Sample PA, Zangwill LM. Rates of retinal nerve fiber layer thinning in glaucoma suspect eyes. Ophthalmology. 2014 7;121(7):1350–8. doi: 10.1016/j.ophtha.2014.01.017. Epub 2014 Mar 13. [PubMed: 24629619]
40. Girkin CA, McGwin G Jr, Sinai MJ, Sekhar GC, Fingeret M, Wollstein G, Varma R, Greenfield D, Liebmann J, Araie M, Tomita G, Maeda N, Garway-Heath DF. Variation in optic nerve and macular structure with age and race with spectral-domain optical coherence tomography. Ophthalmology. 2011 12;118(12):2403–8. doi: 10.1016/j.ophtha.2011.06.013. Epub 2011 Sep 9. [PubMed: 21907415]
41. Poon LY, Antar H, Tsikata E, et al. Effects of Age, Race, and Ethnicity on the Optic Nerve and Peripapillary Region Using Spectral-Domain OCT 3D Volume Scans. Transl Vis Sci Technol. 2018;7(6):12. Published 2018 Nov 27. doi:10.1167/tvst.7.6.12
42. Khoueir Z, Jassim F, Poon LY, et al. Diagnostic Capability of Peripapillary Three-dimensional Retinal Nerve Fiber Layer Volume for Glaucoma Using Optical Coherence Tomography Volume Scans. Am J Ophthalmol. 2017;182:180–193. doi:10.1016/j.ajo.2017.08.001 [PubMed: 28807732]
43. Leung CK, Choi N, Weinreb RN, et al. Retinal nerve fiber layer imaging with spectral-domain optical coherence tomography: pattern of RNFL defects in glaucoma. Ophthalmology. 2010;117(12):2337–2344. doi:10.1016/j.ophtha.2010.04.002 [PubMed: 20678802]
44. Nakatani Y, Higashide T, Ohkubo S, Takeda H, Sugiyama K. Evaluation of macular thickness and peripapillary retinal nerve fiber layer thickness for detection of early glaucoma using spectral domain optical coherence tomography. J Glaucoma. 2011;20(4):252–259. doi:10.1097/IJG.0b013e3181e079ed [PubMed: 20520570]
45. Rao HL, Dasari S, Riyazuddin M, et al. Diagnostic Ability and Structure-function Relationship of Peripapillary Optical Microangiography Measurements in Glaucoma. J Glaucoma. 2018;27(3):219–226. doi:10.1097/IJG.0000000000000873 [PubMed: 29329139]
46. Nouri-Mahdavi K, Hoffman D, Tannenbaum DP, Law SK, Caprioli J. Identifying early glaucoma with optical coherence tomography. Am J Ophthalmol. 2004;137(2):228–235. doi:10.1016/j.ajo.2003.09.004 [PubMed: 14962410]
47. Saito H, Iwase A, Araie M. Comparison of retinal ganglion cell-related layer asymmetry between early glaucoma eyes with superior and inferior hemiretina damage. Br J Ophthalmol. 2020 5;104(5):655–659. doi: 10.1136/bjophthalmol-2019-314563. Epub 2019 Aug 21. [PubMed: 31434647]
48. Yousefi S, Mahmoudi Nezhad GS, Pourahmad S, Vermeer KA, Lemij HG. Distribution and Rates of Visual Field Loss across Different Disease Stages in Primary Open-Angle Glaucoma. Ophthalmol Glaucoma. 2018 Jul-Aug;1(1):52–60. doi: 10.1016/j.ogla.2018.05.005. Epub 2018 Jul 3. [PubMed: 32672633]
49. Nousome D, Mckean-Cowdin R, Richter GM, Burkemper B, Torres M, Varma R, Jiang X. Retinal Nerve Fiber Layer Thickness in Healthy Eyes of African, Chinese, and Latino Americans: A Population-based Multiethnic Study. Ophthalmology. 2020 11 17:S0161–6420(20)31107–6. doi: 10.1016/j.ophtha.2020.11.015. Epub ahead of print.
50. Chang R, Chu Z, Burkemper B, et al. Effect of Scan Size on Glaucoma Diagnostic Performance Using OCT Angiography En Face Images of the Radial Peripapillary Capillaries. J Glaucoma. 2019;28(5):465–472. doi:10.1097/IJG.0000000000001216 [PubMed: 30789527]

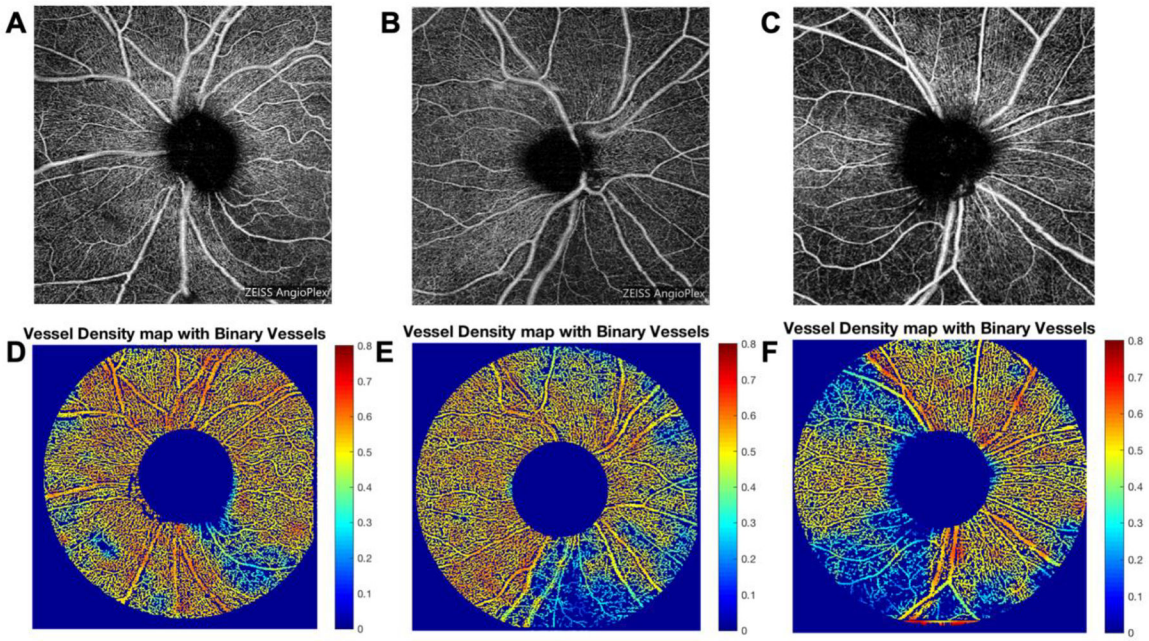

Figure 1: 6×6-mm OCTA *en face* images centered on the ONH of (A) mild, (B) moderate, and (C) severe POAG. Corresponding vessel density map with binary vessels of (D) mild, (E) moderate, and (F) severe POAG.

Areas of higher vessel density are in warmer colors. Abbreviations: OCTA=optical coherence tomography angiography; ONH=optic nerve head; POAG=primary open angle glaucoma.

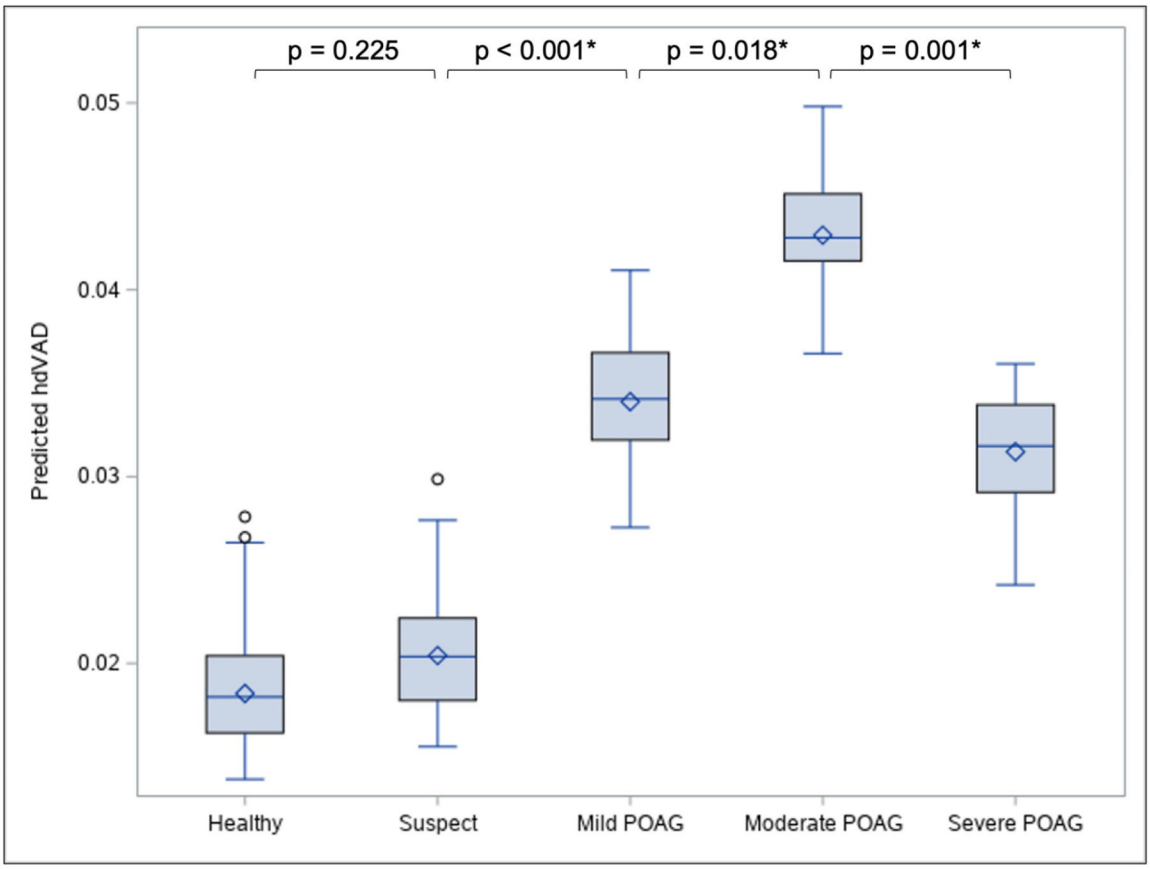

Figure 2: Boxplot illustrating the distribution of age-adjusted predicted hdVAD values across diagnostic groups.

A peak in mean predicted hdVAD (diamond symbol) is observed at moderate POAG, such that its predicted hdVAD is significantly higher than the predicted hdVAD of its flanking diagnostic groups. Circle symbol indicates outlying data point. See Supplemental Figure 1 for distributions and pairwise comparisons of other asymmetry parameters. *Statistically significant ($P < 0.05$), as determined from multivariable linear regression of hdVAD on diagnostic groups controlling for age. Abbreviations: hdVAD=superior and inferior hemiretinal absolute difference in vessel area density; POAG=primary open angle glaucoma.

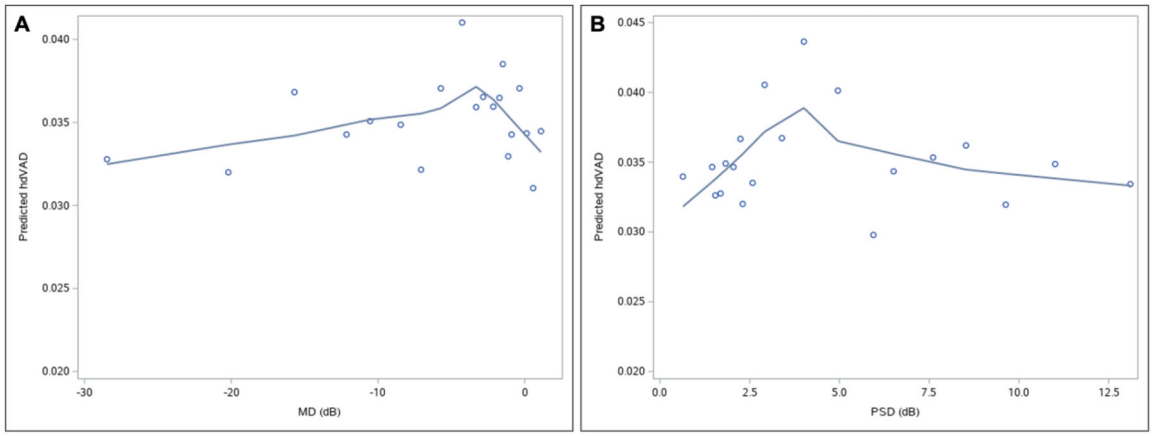

Figure 3: Mean age-adjusted predicted values of hdVAD versus visual field (A) MD and (B) PSD in any POAG.

Plotted data points represent one of the 20 bins created based on percentiles of visual field MD or PSD. Qualitative peaks in hdVAD are observed in the LOWESS regression curve at visual field MD of approximately −4.5 dB and PSD of approximately 4.0 dB, representing relatively early glaucoma. Abbreviations: hdVAD=superior and inferior hemiretinal absolute difference in vessel area density; MD=mean deviation; PSD=pattern standard deviation; POAG=primary open angle glaucoma.

Table 1:

Demographic and ocular characteristics of healthy, glaucoma suspect, and POAG groups.

			POAG [a]				P-Value [b]		
	Healthy[a]	Suspect[a]	Mild	Moderate	Severe	Any	Healthy vs. Suspect	Healthy vs. Any POAG	Suspect vs. Any POAG
n	587	270	67	54	65	186			
Age	56.7 (10.3)	57.7 (10.7)	64.5 (12.1)	66.0 (10.4)	66.9 (11.8)	65.8 (11.5)	0.172	<0.001*	<0.001*
Female Gender	366 (62%)	133 (49%)	30 (45%)	25 (46%)	24 (37%)	79 (42%)	<0.001*	<0.001*	0.168
Hypertension	321 (55%)	107 (40%)	36 (54%)	21 (39%)	30 (46%)	87 (47%)	<0.001*	<0.001*	0.602
Diabetes Mellitus	121 (21%)	31 (11%)	10 (15%)	11 (20%)	16 (25%)	37 (20%)	<0.001*	0.322	0.011*
CDR	0.4 (0.2)	0.6 (0.2)	0.7 (0.1)	0.7 (0.2)	0.9 (0.1)	0.8 (0.2)	<0.001*	<0.001*	<0.001*
MD (dB)	−0.9 (2.7)	−1.4 (2.3)	−1.5 (3.4)	−5.9 (5.6)	−11.3 (8.7)	−6.2 (7.5)	0.057	<0.001*	<0.001*
PSD (dB)	2.3 (1.7)	2.2 (1.7)	2.1 (0.9)	5.1 (3.2)	7.1 (3.6)	4.7 (3.5)	0.582	<0.001*	<0.001*
IOP (mm Hg)	15.1 (2.9)	15.4 (3.9)	15.4 (4.8)	14.1 (4.3)	15.5 (7.0)	15.1 (5.6)	0.168	0.880	0.366

[a] Data listed as mean (standard deviation) or frequency (percent).

[b] For between-group comparisons of age, p-values were determined from logistic regression of diagnostic groups on age. For between-group comparisons of the remaining demographic and ocular characteristics, p-values were determined from logistic regression of diagnostic groups on characteristics with age as a covariate.

* Statistically significant ($P < 0.05$).

Abbreviations: POAG=primary open angle glaucoma; CDR=cup-to-disc ratio; VF MD=visual field mean deviation; PSD=pattern standard deviation; IOP=intraocular pressure.

Table 2:

Mean predicted values of asymmetry, OCTA, and OCT parameters by diagnosis.

	Healthy[a]	Suspect[a]	POAG[a]			
			Mild	Moderate	Severe	Any
Asymmetry Parameters						
hdVAD	0.018 (0.017)	0.020 (0.018)	0.034 (0.025)*	0.043 (0.036)*	0.031 (0.027)*	0.036 (0.029)*
qdVAD	0.025 (0.024)	0.029 (0.028)	0.037 (0.030)*	0.059 (0.047)*	0.043 (0.035)	0.046 (0.038)*
qdRNFL	13.5 (10.1)	14.9 (16.7)	13.8 (14.4)	15.4 (13.7)	12.7 (8.7)	13.9 (12.6)
VAD Parameters						
gVAD	0.348 (0.043)	0.343 (0.049)	0.292 (0.060)*	0.267 (0.062)*	0.231 (0.071)*	0.264 (0.070)*
Superior Hemiretinal VAD	0.444 (0.035)	0.440 (0.042)	0.401 (0.055)*	0.376 (0.059)*	0.331 (0.082)*	0.370 (0.073)*
Inferior Hemiretinal VAD	0.436 (0.029)	0.431 (0.040)	0.386 (0.055)*	0.350 (0.075)*	0.310 (0.079)*	0.349 (0.076)*
Superior Quadrant VAD	0.471 (0.038)	0.458 (0.047)*	0.420 (0.063)*	0.384 (0.072)*	0.331 (0.090)*	0.379 (0.085)*
Inferior Quadrant VAD	0.483 (0.029)	0.474 (0.043)*	0.429 (0.058)*	0.376 (0.096)*	0.324 (0.092)*	0.377 (0.093)*
RNFL Parameters						
gRNFL	92.2 (10.6)	88.2 (11.0)*	78.2 (10.4)*	73.3 (10.9)*	68.1 (11.4)*	73.7 (11.6)*
Superior Quadrant RNFL	115.0 (16.6)	106.6 (17.831)*	96.2 (18.6)*	85.7 (18.7)*	80.1 (16.9)*	88.3 (19.3)*
Inferior Quadrant RNFL	122.5 (18.3)	112.8 (21.5)*	95.0 (20.3)*	86.1 (24.7)*	73.5 (17.7)*	85.9 (22.6)*
Visual Field Parameters						
Visual Field Mean Deviation	−0.94 (2.67)	−1.39 (2.27)	−1.49 (3.38)	−5.88 (5.64)*	−11.25 (8.67)*	−6.17 (7.53)*
Pattern Standard Deviation	2.28 (1.66)	2.21 (1.61)	2.06 (0.89)	5.13 (3.22)*	7.11 (3.57)*	4.69 (3.50)*

[a]Data listed as mean (standard deviation).

*Statistically significantly different ($P < 0.05$) than healthy, as determined from age-adjusted multivariable linear regression of ocular parameter on diagnostic groups.

Abbreviations: OCTA=optical coherence tomography angiography; OCT=optical coherence tomography; POAG=primary open angle glaucoma; hdVAD=superior and inferior hemiretinal absolute difference in vessel area density; qdVAD=superior and inferior quadrant absolute difference in vessel area density; qdRNFL=superior and inferior quadrant absolute difference in retinal nerve fiber layer thickness; VAD=vessel area density; gVAD=global vessel area density; RNFL=retinal fiber layer thickness; gRNFL=average global retinal nerve fiber layer thickness.

Table 3:

Diagnostic accuracy of age-adjusted OCTA and OCT parameters based on AUC for distinguishing each diagnostic group from healthy.

	Suspect	POAG			
		Mild	Moderate	Severe	Any
Asymmetry Parameters					
hdVAD	0.517	0.685	0.681	0.594	0.656
qdVAD	0.519	0.611	0.725	0.630	0.648
qdRNFL	0.488	0.473	0.525	0.497	0.497
VAD and RNFL Parameters					
gVAD	0.522	0.720	0.828	0.894	0.804
Superior Hemiretinal VAD	0.579	0.697	0.832	0.872	0.789
Inferior Hemiretinal VAD	0.546	0.737	0.797	0.907	0.806
gRNFL	0.602	0.793	0.855	0.914	0.847
Combined Parameters					
hdVAD + gRNFL	0.603	0.818*	0.866	0.914	0.859*
qdVAD + gRNFL	0.602	0.795	0.881	0.914	0.855
qdRNFL + gRNFL	0.604	0.794	0.873	0.915	0.852
gVAD + gRNFL	0.613	0.786	0.866	0.931	0.851

*Statistically significantly higher ($P < 0.05$) than AUC of gRNFL alone for distinguishing the same diagnostic group from healthy, as determined by DeLong's test.

Abbreviations: OCTA=optical coherence tomography angiography; OCT=optical coherence tomography; AUC=area under receiver operating curve; POAG=primary open angle glaucoma; hdVAD=superior and inferior hemiretinal absolute difference in vessel area density; qdVAD=superior and inferior quadrant absolute difference in vessel area density; qdRNFL=superior and inferior quadrant absolute difference in retinal nerve fiber layer thickness; VAD=vessel area density; RNFL=retinal nerve fiber layer thickness; gVAD=global vessel area density; gRNFL=average global retinal nerve fiber layer thickness.